Electrodeposited Germanium Nanowires

Naveen K. Mahenderkar,[†] Ying-Chau Liu,[‡] Jakub A. Koza,[‡] and Jay A. Switzer[‡,*]

[†]Department of Materials Science and Engineering and Graduate Center for Materials Research, Missouri University of Science and Technology, Rolla, Missouri 65409-1170, United States, and [‡]Department of Chemistry and Graduate Center for Materials Research, Missouri University of Science and Technology, Rolla, Missouri 65409-1170, United States

ABSTRACT Germanium (Ge) is a group IV semiconductor with superior electronic properties compared with silicon, such as larger carrier mobilities and smaller effective masses. It is also a candidate anode material for lithium-ion batteries. Here, a simple, one-step method is introduced to electrodeposit dense arrays of Ge nanowires onto indium tin oxide (ITO) substrates from aqueous solution. The electrochemical reduction of ITO produces In nanoparticles that act as a reduction site for aqueous Ge(IV) species, and as a solvent for the crystallization of Ge nanowires. Nanowires deposited at 95 °C have an average diameter of 100 nm, whereas those deposited at room temperature have an average diameter of 35 nm. Both optical absorption and Raman spectroscopy suggest that the electrodeposited Ge is degenerate. The material has an indirect bandgap of 0.90–0.92 eV, compared with a value of 0.67 eV for bulk, intrinsic Ge. The blue shift is attributed to the Moss–Burstein effect, because the material is a p-type degenerate semiconductor. On the basis of the magnitude of the blue shift, the hole concentration is estimated to be 8×10^{19} cm^{-3}. This corresponds to an In impurity concentration of about 0.2 atom %. The resistivity of the wires is estimated to be 4×10^{-5} Ω·cm. The high conductivity of the wires should make them ideal for lithium-ion battery applications.

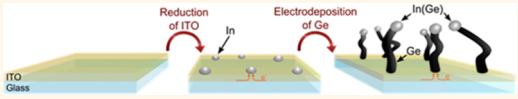

KEYWORDS: germanium nanowires · electrodeposition · Moss–Burstein shift · degenerate semiconductor · indium nanoparticles

Germanium (Ge) is a group IV semiconductor material that was used in the first transistor prior to silicon (Si).[1] It has twice the electron mobility (3900 cm^2/(V s)), four times the hole mobility (1900 cm^2/(V s)), a larger exciton Bohr radius (24 nm), and a lower hole effective mass ($0.28m_o$) compared with Si.[2,3] Because of its high carrier mobility, Ge is being considered as a replacement for Si as the active channel material for CMOS transistors.[4–6] Ge is also an attractive anode material for Li-ion batteries, because it has a larger theoretical charge–discharge capacity than graphite.[7,8] However, it undergoes a 370% change in volume, leading to fragmentation and loss of electrical contact in bulk electrodes.[9] Nanostructures of Ge have been shown to accommodate the large volumetric changes during Li intercalation.[7,10–12] The room temperature (RT) diffusivity of Li in Ge is 400 times higher than that in Si, indicating that Ge may be an attractive electrode material for high-power-rate anodes.[13] Nanowires of Ge grown using various methods showed a discharge capacity in the range of 600–1140 mA·h/g.[14,15] Despite its superior properties, the lack of inexpensive and simple methods to produce nanostructured Ge has limited its use. Electrodeposition of Ge from aqueous solution is thermodynamically not feasible, and in practice the growth is restricted to a few monolayers due to the competing reduction of water to hydrogen gas.[16–19] Recently, Maldonado and co-workers electrodeposited nanostructures of Ge from aqueous solutions on various metallic liquids (Hg, Ga and In) using a new route that they call the electrochemical liquid–liquid–solid (ec-LLS) process.[14,20–22] This process utilizes a metallic liquid electrode that acts both as an electrode for electrodeposition and as a solvent for recrystallization. Nanostructured filaments of Ge on liquid Hg,[20] Ge nanowires on In nanoparticles,[14] and epitaxial Ge nanowires on Ga nanodroplets[21,22] were electrodeposited. Here, we show a simple one-step method to grow dense arrays of Ge nanowires utilizing the ec-LLS process directly on indium–tin oxide (ITO) substrates from aqueous solution. The electrochemical reduction of ITO decorates the substrate with In nanoparticles, which act both as a reduction site for dissolved Ge species and as a solvent for crystallization of the Ge nanowires.

RESULTS AND DISCUSSION

The reaction scheme we use to produce the Ge nanowires on ITO substrates is shown in Figure 1. The electrochemical reduction of ITO decorates the substrate with In nanoparticles,

* Address correspondence to jswitzer@mst.edu.

Received for review July 10, 2014 and accepted August 26, 2014.

Published online August 26, 2014
10.1021/nn503784d

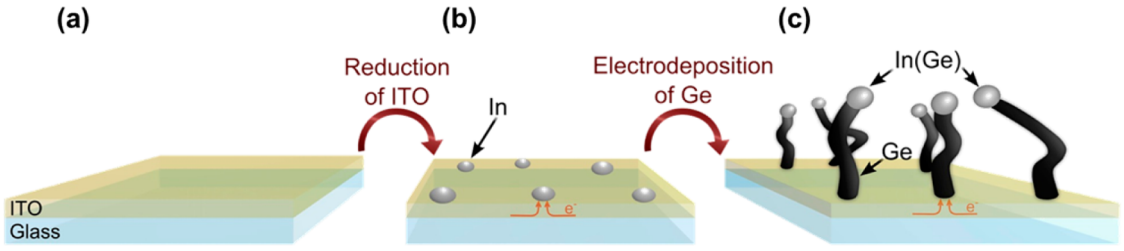

Figure 1. Schematic of electrodeposition of Ge nanowires. (a) The as-received ITO in an aqueous electrolyte of Ge(IV). (b) Electrochemical reduction of ITO to In nanoparticles dispersed evenly over the entire surface of ITO. (c) Ge nanowires grow on ITO with In nanoparticles at the tip of the nanowires.

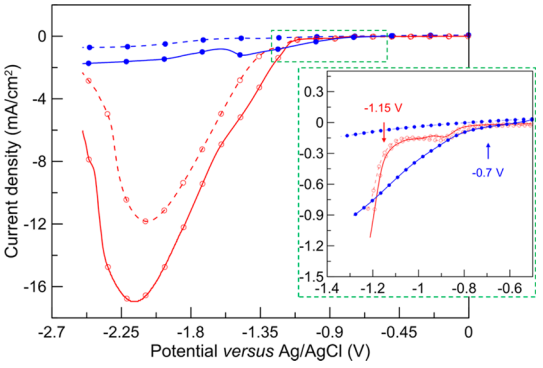

Figure 2. Electrochemical data for Ge nanowire electrodeposition. Linear sweep voltammograms for the reduction of ITO and Ge nanowire deposition. Solid lines are the linear scans of ITO in a solution with 50 mM Ge(IV) and the dashed lines are without Ge(IV). Lines with hollow circles are the first scans, and lines with solid circles are the second scans. The scans were performed from 0 to −2.5 V *versus* Ag/AgCl at 100 mV/s. Inset shows the magnified view of the onset reduction potentials.

which act both as a reduction site for dissolved Ge(IV) species and as a solvent for crystallization of the nanowires. The dissolved Ge(IV) species are initially reduced to Ge(s) followed by dissolution into the In nanoparticles. Continuous reduction and dissolution leads to saturation of Ge in In, leading to the crystallization of Ge nanowires. Electrochemical reduction of ITO forms an In nanoparticle on the surface (Figure 1b). The In nanoparticle in contact with the ITO acts as the electrode for the reduction of Ge(IV) and also dissolves the reduced Ge into the particle. Upon reaching saturation, the Ge starts to crystallize out of the nanoparticle allowing the growth of the nanowire (Figure 1c). A key to the reaction scheme is that ITO electrochemically reduces to In at a potential very similar to the potential at which Ge(IV) is reduced to Ge at the In nanoparticles.

The electrochemical reduction of ITO and formation of In nanoparticles was studied using linear sweep voltammetry. Figure 2 shows the current−potential responses of ITO in the solution, both without (dashed line) and with (solid line) aqueous Ge(IV). All of the potentials in the article are *versus* Ag/AgCl/sat. KCl. A significant increase in current density occurs at −1.15 V during the first scan of ITO in the solution without Ge(IV) (open circle dashed line). This increase in current density is due to the reduction of ITO to In nanoparticles. The electrochemical reduction of ITO to In nanoparticles was also reported by Huang *et al.*[23] During the second scan (solid circle dashed line), the current density increase is very minimal, indicating an almost complete reduction of ITO and surface coverage with In nanoparticles.

The first cathodic scan with Ge(IV) (open circle, solid line) in the solution shows an increase in the current density nearly at the same potential of −1.15 V. This indicates that the presence of Ge(IV) in the solution did not affect the potential at which ITO reduces. However, during the second scan (solid circle, solid line), the current density increase occurs at a more positive potential of −0.7 V, indicating the reduction of Ge(IV) due to the presence of In on the surface of ITO. The ITO in a Ge(IV) solution shows no evidence of Ge deposition at potentials positive of −1.15 V. On the contrary, a reduced ITO (with In nanoparticles) shows an increase in current density at potentials between −0.7 and −1.15 V, indicating that reduction of Ge(IV) occurs exclusively at the In nanoparticles. An In(s) foil used as a working electrode also showed a reduction current at nearly the same potential (−0.79 V) as that for the In nanoparticles, confirming that Ge(IV) reduction occurs on In (Supporting Information, Figure S1). The single-step growth of Ge nanowires occurs mainly due to the reduction potential of ITO being very similar to that of reduction of Ge(IV) on In (see Figure 2 inset). The poor electrocatalytic activity of In for H^+ reduction enables continuous reduction of Ge(IV) over the nanoparticle surface.[24] As a result, the potential in a single solution can be controlled to reduce the ITO prior to the deposition of Ge nanowires. All of the nanowire samples for further investigations are prepared by applying −1.3 V for 10 min. The deposits are thoroughly rinsed with deionized water and dried in air prior to analysis. The as-prepared samples appear dark black in color and eventually become light gray after a prolonged (1−2 months) exposure to a lab atmosphere.

The Ge deposition was also probed by X-ray diffraction (XRD). The XRD pattern of the ITO shows strong reflections of In_2O_3, with no evidence of In (Figure 3a).

The reduced ITO, however, shows reflections of both ITO and In (Figure 3b). This shows that the spherical particles formed on the surface of ITO are In. Using the Scherrer equation,[25] we estimate an average X-ray coherence length of 60 nm for the In nanoparticles. To study the effect of deposition temperature, the nanowires were deposited at 95 °C and RT. Ge nanowires at both of the deposition temperatures show strong XRD peaks for crystalline Ge (Figures 3c and 3d). The line broadening in XRD of the Ge deposits gives an average crystallite size of 50 nm for Ge deposited at 95 °C and 30 nm for the Ge deposited at room temperature. Precision lattice parameters determined using the Nelson–Riley extrapolation[26] applied to the pattern of reflections (Supporting Information, Figure S2) are

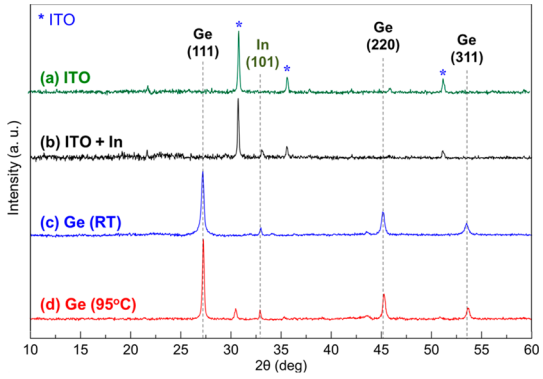

Figure 3. Crystallinity of Ge nanowires. X-ray diffraction patterns of ITO (a), reduced ITO (b), and Ge nanowires deposited at room temperature (c) and 95 °C (d). Ge reflections are indicated as black dashed vertical lines (JCPDS card no. 4-0545); asterisks stand for the ITO substrate.

5.6582 Å (for 95 °C) and 5.6707 Å (for RT). These are both in good agreement with the expected lattice parameter of 5.6579 Å for bulk Ge.[27,28]

The morphology of as-received ITO (inset of Figure 4a) is smooth and does not show any evidence of elemental In on the surface. The reduced ITO shows numerous, uniformly dispersed, relatively spherical In nanoparticles (Figure 4a,d). An average In particle size of 50 nm for RT (Figure 4b) and 100 nm for 95 °C reduction (Figure 4c) is observed. The presence of both ITO and the In nanoparticles suggests that incomplete reduction occurred. This enables electrical contact to the In nanoparticles for the reduction of Ge(IV). It is also evident from the size distribution that with increase in temperature of reduction, the nanoparticle size increases. Figure 4e shows the Ge nanowires deposited at room temperature and Figure 4h shows the Ge nanowires produced at 95 °C. An average nanowire diameter of 35 nm (Figure 4f) for the room temperature deposit and 100 nm (Figure 4g) for the 95 °C deposit is observed. The size of the In nanoparticles and the Ge nanowire diameters are comparable. That is, large nanoparticles yield large-diameter nanowires. A spaghetti-like morphology is evident for both the deposition temperatures. A dense array of Ge nanowires can be deposited directly onto an ITO substrate at ambient conditions. Figure 4i shows the cross section of the nanowires deposited at 95 °C.

Figure 5a shows a transmission electron microscope (TEM) image of a Ge nanowire with an In nanoparticle at the tip of the wire that was deposited at 95 °C. Energy dispersive X-ray spectroscopy (EDS) performed

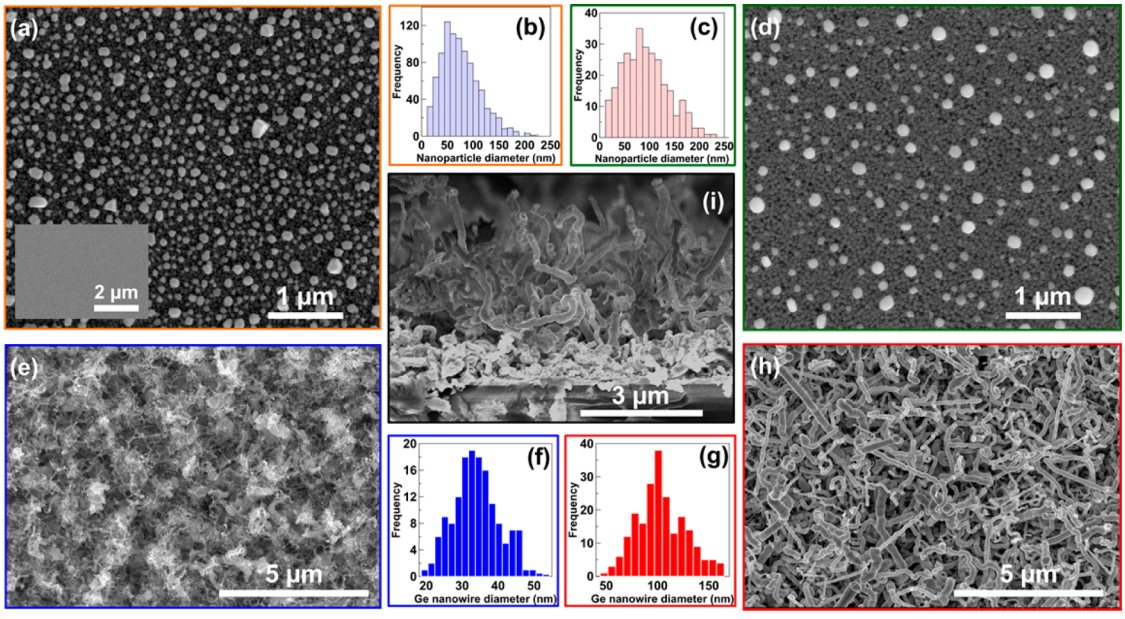

Figure 4. Morphology of In nanoparticles and Ge nanowires. SEM of ITO reduced at room temperature (a) with an average particle size of 50 nm (b) and the ITO reduced at 95 °C (d) with an average particle size of 100 nm (c). The inset in (a) shows the as-received ITO prior to reduction. Ge nanowires deposited at room temperature (e) with an average nanowire diameter of 35 nm (f) and deposited at 95 °C (h) with an average diameter of 100 nm (g). Cross section of nanowires deposited at 95 °C (i).

on both the In tip (Figure 5b) and the Ge nanowire (Figure 5c) verify the compositions of the Ge wire and the In tip. The EDS of the In nanoparticle tip shows a composition of *ca.* 20 atom % Ge and 80 atom % In. The presence of Ge in In implies the dissolution of Ge in In during the reduction of Ge(IV). EDS of the nanowire shows that it is predominately Ge with a small amount (0.14 ± 0.04 atom %) of In. The inset in Figure 5a is the electron diffraction of the nanowire with a polycrystalline spot pattern. The variations in contrast along the nanowire also suggest that the nanowire is polycrystalline, in agreement with the XRD patterns. It is also evident that the In nanoparticle stays on top of the nanowire while the ITO provides the electrical contact. Figure 5d shows a high-resolution TEM image of the nanowire deposited at 95 °C. Figure 5e shows the diffractogram of the high-resolution image shown in Figure 5d. The spots in the diffractogram reveal the direction of growth and the *d*-spacing value. Figure 5f is a reconstructed high-resolution TEM image of the same nanowire from the diffractogram. The spacing between the lattice planes is measured to be 3.26 Å, in agreement with the spacing of (111) planes for diamond cubic Ge.

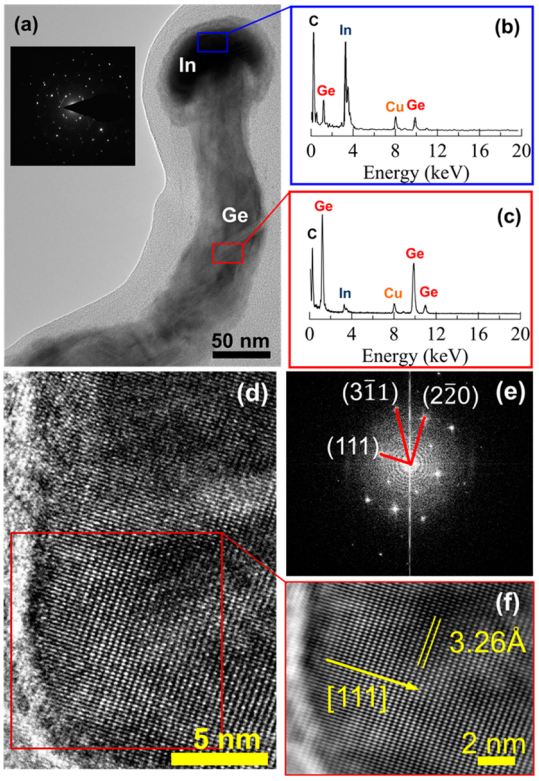

Figure 5. (a) TEM of a single Ge nanowire deposited at 95 °C with an In nanoparticle at the tip of the wire. Inset shows the selected area electron diffraction pattern of the nanowire. EDS spectrum with the compositions of In nanoparticle (b) and Ge nanowire (c). (d) High-resolution TEM of Ge nanowire, (e) diffractogram corresponding to the high-resolution TEM image in (d), and (f) reconstructed high-resolution image with the (111) *d*-spacing and the [111] direction indicated.

The bandgap of an electrodeposited Ge was estimated from a plot of square root of absorbance *versus* photon energy (Figure 6a). As described in the Supporting Information (Supporting Information, Figure S3), the absorbance was corrected for scattering of the light by the Ge nanowires. The linear plots in Figure 6a are consistent with an indirect bandgap.[2] The transition in Ge is indirect due to the position of the conduction band minimum at the L symmetry point of the Brillouin zone edge and the valence band maximum at the Γ symmetry point of the Brillouin zone center. The indirect transition process involves a photon and also a phonon that is either emitted or absorbed in the excitation event. The phonon energy in an indirect transition is normally on the order of 0.01 eV, so the intercept is a close approximation to the actual bandgap of the nanowires. An optical bandgap of 0.92 eV (for 95 °C) and 0.90 eV (for RT) is observed from the absorbance data. Ge has an intrinsic bandgap

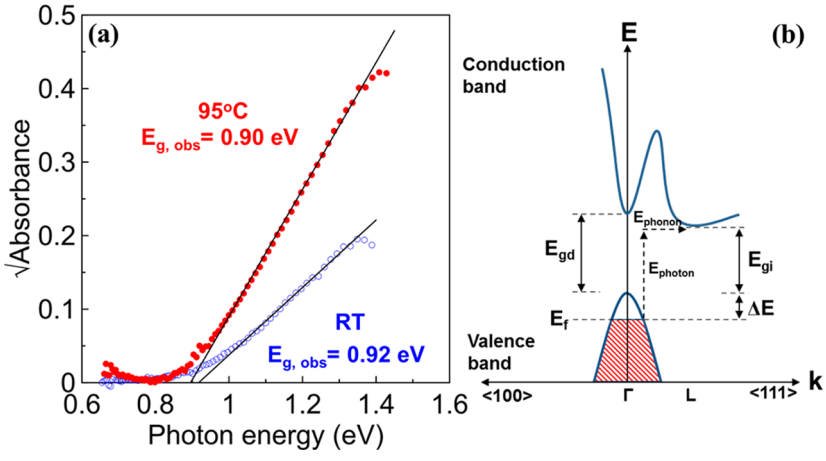

Figure 6. Optical bandgap measurements of Ge nanowires. (a) Square root of absorbance as a function of photon energy for Ge nanowires deposited at 95 °C (red solid circle) and room temperature (blue hollow circle). The energy-intercept of the fit to the linear region of the curve is the indirect bandgap. (b) Schematic diagram of the band structure for a degenerate p-Ge. The increase in energy (Δ*E*) is the Moss−Burstein shift due to the high carrier concentration.

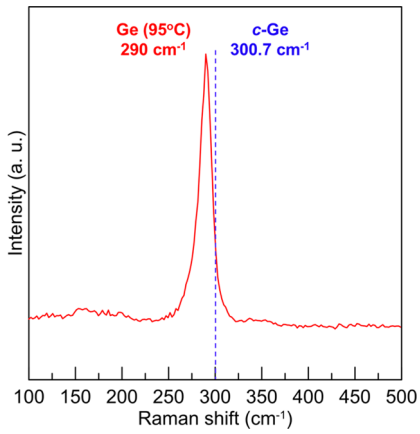

Figure 7. Raman spectrum of Ge nanowires deposited at 95 °C (red solid line); the blue dashed line corresponds to the first-order Stokes peak for crystalline bulk Ge.

of 0.67 eV, which gives a blue shift (ΔE) of 0.25 eV (for 95 °C) and 0.23 eV (for RT). Although a blue shift is expected for quantum confinement in nanoscale materials, the size of our nanowires is too large to account for this large shift. We attribute the blue shift to the fact that the electrodeposited Ge is doped with In to degeneracy. Indium is a p-type dopant for Ge. If the doping density is very high, the Fermi level can be shifted to an energy below the valence band. Figure 6b shows the schematic diagram of the band structure for a degenerate p-Ge. The shift of Fermi energy due to high carrier concentration can result in a blue shift in the absorption spectrum, known as the Moss–Burstein shift.[2,29] The carrier density can be estimated from the blue shift using the Moss–Burstein equation (eq 1).

$$\Delta E(\text{eV}) = E_f - E_v = \frac{\hbar^2(3\pi^2 n)^{2/3}}{2m_h^*} \quad (1)$$

Here, ΔE is the Moss–Burstein shift; E_f is the Fermi energy level; E_v is the energy at the top of valence band; $\hbar$ is the reduced Planck's constant; m_h^* is the effective hole mass, and n is the charge carrier density. With eq 1, the hole densities are calculated to be 8.4×10^{19} cm^{-3} (for 95 °C) and 7.4×10^{19} cm^{-3} (for RT). The optical bandgap and the carrier densities of the nanowires for both of the deposition temperatures are nearly the same within the experimental error of the measurement.

The Ge nanowire sample was also probed using Raman spectroscopy to study the effect of carrier concentration and nanowire size on the Raman shift. The first-order Stokes peak for bulk crystalline Ge occurs at 300.7 cm^{-1}.[30] Several groups have studied the effect of carrier concentration (phonon-plasmon coupling),[31,32] and crystal and nanowire size (phonon confinement effect) on the Raman shift.[33,34] Contributions from any of these effects cause a redshift and broadening of the Raman peaks. The Ge nanowires deposited at 95 °C show a redshift of *ca.* 10 cm^{-1}, with the peak of Ge shifted to 290 cm^{-1} (Figure 7). The blue dashed line in Figure 7 shows the first-order Stokes peak for bulk crystalline Ge and the red solid spectrum corresponds to the Ge nanowires deposited at 95 °C. This characteristic redshift for the nanowires is attributed to the presence of a high carrier concentration in the nanowires, consistent with a previous study by Cerdeira and Cardona.[32] We assume that the crystallite size and nanowire diameter are too large compared to the Bohr radius of Ge (24 nm) to show significant red shifts due to the phonon confinement effect.

The hole concentrations calculated from eq 1 can be used to estimate the In concentration in the Ge. The unit cell of Ge has a volume of 1.799×10^{-22} cm^3, and contains 8 Ge atoms. There are, therefore, 4.455×10^{22} Ge atoms per cm^3. If we assume that each hole in the material results from one substitutional In atom, the concentration of In in the Ge is 0.16 atom % for the wires grown at room temperature and 0.18 atom % for the wires grown at 95 °C. These calculated In concentrations agree well with the In content of 0.14 ± 0.04 atom % that was measured by EDS in the TEM for the Ge nanowire grown at 95 °C. We can also estimate the resistivity of the Ge nanowires based on the measured hole concentrations and the known bulk mobility of holes in Ge. The calculated resistivity is 3.8×10^{-5} Ω·cm (for 95 °C) and 4.4×10^{-5} Ω·cm (for RT). This indicates that the nanowires have a very high conductivity enabling the growth of long Ge nanowires, even at room temperature. Hence, the electrodeposited Ge nanowires may be too highly doped for conventional electronic applications, but they should be ideal as a high-capacity anode material for lithium ion batteries.

CONCLUSIONS

In summary, we have demonstrated the electrodeposition of crystalline Ge nanowires at room temperature by direct electroreduction of ITO in a single-step from aqueous solution. The similarity of the reduction potentials of ITO and Ge(IV) enables this single-step potentiostatic growth of Ge nanowires. The nanowires are deposited at 95 °C and room temperature, and the effect of temperature on the crystallinity, nanowire diameter, crystal size, and optical bandgap is examined. The nanowires deposited at both temperatures are polycrystalline. The grain size and the nanowire diameter decrease with a decrease in deposition temperature, consistent with the decrease in the diameter of the initially formed In nanoparticles. The In nanoparticles stay on top of the nanowires during the growth with the ITO at the base providing the electrical contact. The dissolution of Ge in In nanoparticle supports the notion of growth by dissolution and crystallization by the electrochemical liquid–liquid–solid (ec-LLS) mechanism proposed by Madonaldo and co-workers.[14,20–22] The optical bandgap of the material blue shifts due to the high

carrier density (*ca.* 8×10^{19} cm^{-3}). The resistivity of the nanowires is estimated to be very low (*ca.* 4×10^{-5} $\Omega \cdot cm$), enabling the growth of long wires even at room temperature.

MATERIALS AND METHODS

The Ge nanowires were electrodeposited at room temperature and 95 °C from a solution of 50 mM GeO_2, 0.5 M Na_2SO_4, and 0.1 M $C_4H_6O_4$ (succinic acid) with the pH adjusted to 6.5 using NaOH. The same solution without GeO_2 was used for the electrochemical reduction studies of ITO to In nanoparticles. Electrochemical measurements were performed with a potentiostat/galvanostat (EG&G model 273A). A platinum mesh was used as the counter electrode, and an Ag/AgCl/sat. KCl was used as the reference electrode.

The crystallinity of the nanowires was characterized using a high-resolution Philips X-Pert MRD X-ray diffractometer with a Cu $K_{\alpha 1}$ radiation source (λ = 1.5405 Å). The morphology of the films was determined by means of scanning electron microscopy (Helios Nanolab dual beam and Hitachi S4700 field-emission). The transmission electron microscopy and energy dispersive spectroscopy of the nanowires and the In nanoparticles were measured using the Technai F20. Samples for TEM analysis were prepared by etching ITO with Ge nanowires using 1:1 (v/v) HCl solution and sonicating the wires in ethanol for 5 min. The suspension was then drop-cast onto copper grids coated with ultrathin carbon films on holey carbon (Pacific Grid Tech).

The bandgap measurements were performed using a dual beam UV−vis-NIR spectrophotometer (Varian Cary 5). The as-prepared Ge nanowire films were etched using a 1:1 (v/v) HCl solution to dissolve the ITO. A drop of etching solution cast on the nanowire film enabled the etching of ITO without causing the nanowire film to slide off the glass. The glass with nanowires was then dried and used for the absorbance measurements. This ensured that the absorbance was solely due to the nanowires. Raman measurements were carried out using a Horiba Jobin-Yvon LabRam Aramis Microscope with a HeNe laser (λ = 633 nm) as the excitation source with an incident power of 0.5 mW to minimize sample heating. The as-deposited Ge nanowire samples were rinsed using deionized (DI) water, dried in air, and used without any post processing.

Conflict of Interest: The authors declare no competing financial interest.

Supporting Information Available: Chemicals used, reduction studies of Ge(IV) on In(s) foil with SEM and EDS analysis, Nelson−Riley extrapolation for precision lattice parameters, and the correction method for light scattering by the Ge nanowires in the absorption spectrum. This material is available free of charge *via* the Internet at http://pubs.acs.org.

Acknowledgment. This material is based upon work supported by the U.S. Department of Energy, Office of Basic Energy Sciences, Division of Materials Sciences and Engineering, under Grant No. DE-FG02-08ER46518.

REFERENCES AND NOTES

1. Bardeen, J.; Brattain, W. H. The Transistor, a Semi-Conductor Triode. *Phys. Rev.* **1948**, *74*, 230–231.
2. Pankove, J. I. *Optical Processes in Semiconductors*; Dover Publications: New York, 1975.
3. Yu, B.; Sun, X. H.; Calebotta, G. A.; Dholakia, G. R.; Meyyappan, M. One-Dimensional Germanium Nanowires for Future Electronics. *J. Cluster Sci.* **2006**, *17*, 579–597.
4. Chui, C. O.; Ramanathan, S.; Triplett, B. B.; McIntyre, P. C.; Saraswat, K. C. Germanium MOS Capacitors Incorporating Ultrathin High-κ Gate Dielectric. *IEEE Electron Device Lett.* **2002**, *23*, 473–475.
5. Maeda, T.; Ikeda, K.; Nakaharai, S.; Tezuka, T.; Sugiyama, N.; Moriyama, Y.; Takagi, S. High Mobility Ge-on-Insulator p-Channel MOSFETs Using Pt Germanide Schottky Source/Drain. *IEEE Electron Device Lett.* **2005**, *26*, 102–104.
6. Bojarczuk, N. A.; Copel, M.; Guha, S.; Narayanan, V.; Preisler, E. J.; Ross, F. M.; Shang, H. Epitaxial Silicon and Germanium on Buried Insulator Heterostructures and Devices. *Appl. Phys. Lett.* **2003**, *83*, 5443–5445.
7. Graetz, J.; Ahn, C. C.; Yazami, R.; Fultz, B. Nanocrystalline and Thin Film Germanium Electrodes with High Lithium Capacity and High Rate Capabilities. *J. Electrochem. Soc.* **2004**, *151*, A698–A702.
8. Yoon, S.; Park, C.-M.; Sohn, H.-J. Electrochemical Characterizations of Germanium and Carbon-Coated Germanium Composite Anode for Lithium-Ion Batteries. *Electrochem. Solid-State Lett.* **2008**, *11*, A42–A45.
9. Song, T.; Cheng, H.; Town, K.; Park, H.; Black, R. W.; Lee, S.; Park, W. I.; Huang, Y.; Rogers, J. A.; Nazar, L. F.; *et al.* Electrochemical Properties of Si-Ge Heterostructures as an Anode Material for Lithium Ion Batteries. *Adv. Funct. Mater.* **2014**, *24*, 1458–1464.
10. Lee, H.; Kim, M. G.; Choi, C. H.; Sun, Y.-K.; Yoon, C. S.; Cho, J. Surface-Stabilized Amorphous Germanium Nanoparticles for Lithium-Storage Material. *J. Phys. Chem. B* **2005**, *109*, 20719–20723.
11. Rudawski, N. G.; Darby, B. L.; Yates, B. R.; Jones, K. S.; Elliman, R. G.; Volinsky, A. A. Nanostructured Ion Beam-Modified Ge Films for High Capacity Li Ion Battery Anodes. *Appl. Phys. Lett.* **2012**, *100*, 083111.
12. Park, M. H.; Kim, K.; Kim, J.; Cho, J. Flexible Dimensional Control of High-Capacity Li-Ion-Battery Anodes: From 0D Hollow to 3D Porous Germanium Nanoparticle Assemblies. *Adv. Mater.* **2010**, *22*, 415–418.
13. Chan, C. K.; Zhang, X. F.; Cui, Y. High Capacity Li Ion Battery Anodes Using Ge Nanowires. *Nano Lett.* **2007**, *8*, 307–309.
14. Gu, J.; Collins, S. M.; Carim, A. I.; Hao, X.; Bartlett, B. M.; Maldonado, S. Template-Free Preparation of Crystalline Ge Nanowire Film Electrodes *via* an Electrochemical Liquid-Liquid-Solid Process in Water at Ambient Pressure and Temperature for Energy Storage. *Nano Lett.* **2012**, *12*, 4617–4623.
15. Kennedy, T.; Mullane, E.; Geaney, H.; Osiak, M.; O'Dwyer, C.; Ryan, K. M. High-Performance Germanium Nanowire-Based Lithium-Ion Battery Anodes Extending Over 1000 Cycles through *in Situ* Formation of a Continuous Porous Network. *Nano Lett.* **2014**, *14*, 716–723.
16. Hall, J. I.; Koenig, A. E. Electrochemical Properties of Germanium. *Trans. Electrochem. Soc.* **1934**, *65*, 215–219.
17. Szekely, G. Electrodeposition of Germanium. *J. Electrochem. Soc.* **1951**, *98*, 318–324.
18. Liang, X.; Jayaraju, N.; Stickney, J. L. Aqueous Ge Atomic Layer Deposition on Au. *ECS Trans.* **2007**, *11*, 249–258.
19. Liang, X.; Kim, Y. G.; Gebergziabiher, D. K.; Stickney, J. L. Aqueous Electrodeposition of Ge Monolayers. *Langmuir* **2010**, *26*, 2877–2884.
20. Carim, A. I.; Collins, S. M.; Foley, J. M.; Maldonado, S. Benchtop Electrochemical Liquid−Liquid−Solid Growth of Nanostructured Crystalline Germanium. *J. Am. Chem. Soc.* **2011**, *133*, 13292–13295.
21. Fahrenkrug, E.; Gu, J.; Jeon, S.; Veneman, P. A.; Goldman, R. S.; Maldonado, S. Room-Temperature Epitaxial Electrodeposition of Single-Crystalline Germanium Nanowires at the Wafer Scale from an Aqueous Solution. *Nano Lett.* **2014**, *14*, 847–852.
22. Ma, L.; Gu, J.; Fahrenkrug, E.; Maldonado, S. Electrochemical Liquid-Liquid-Solid Deposition of Crystalline Ge Nanowires as a Function of Ga Nanodroplet Size. *J. Electrochem. Soc.* **2014**, *161*, D3044–D3050.
23. Huang, C. A.; Li, K. C.; Tu, G. C.; Wang, W. S. The Electrochemical Behavior of Tin-Doped Indium Oxide During Reduction in 0.3 M Hydrochloric Acid. *Electrochim. Acta* **2003**, *48*, 3599–3605.

24. Butler, J. N.; Dienst, M. Hydrogen Evolution at a Solid Indium Electrode. *J. Electrochem. Soc.* **1965**, *112*, 226–232.
25. Patterson, A. The Scherrer Formula for X-Ray Particle Size Determination. *Phys. Rev.* **1939**, *56*, 978–982.
26. Nelson, J. B.; Riley, D. P. An Experimental Investigation of Extrapolation Methods in the Derivation of Accurate Unit-Cell Dimensions of Crystals. *Proc. Phys. Soc.* **1945**, *57*, 160.
27. Baker, J. F. C.; Hart, M. An Absolute Measurement of the Lattice Parameter of Germanium Using Multiple-Beam X-Ray Diffractometry. *Acta Crystallogr., Sect. A* **1975**, *31*, 364–367.
28. Cooper, A. Precise Lattice Constants of Germanium, Aluminum, Gallium Arsenide, Uranium, Sulphur, Quartz and Sapphire. *Acta Crystallogr.* **1962**, *15*, 578–582.
29. Burstein, E. Anomalous Optical Absorption Limit in InSb. *Phys. Rev.* **1954**, *93*, 632–633.
30. Parker, J. H., Jr.; Feldman, D. W.; Ashkin, M. Raman Scattering by Silicon and Germanium. *Phys. Rev.* **1967**, *155*, 712–714.
31. Sanson, A.; Giarola, M.; Napolitani, E.; Impellizzeri, G.; Privitera, V.; Carnera, A.; Mariotto, G. Study of Carrier Concentration Profiles in Al-Implanted Ge by Micro-Raman Spectroscopy under Different Excitation Wavelengths. *J. Raman Spectrosc.* **2013**, *44*, 1097–4555.
32. Cerdeira, F.; Cardona, M. Effect of Carrier Concentration on the Raman Frequencies of Si and Ge. *Phys. Rev. B* **1972**, *5*, 1440–1454.
33. Jalilian, R.; Sumanasekera, G. U.; Chandrasekharan, H.; Sunkara, M. K. Phonon Confinement and Laser Heating Effects in Germanium Nanowires. *Phys. Rev. B* **2006**, *74*, 155421.
34. Wang, X.; Shakouri, A.; Yu, B.; Sun, X.; Meyyappan, M. Study of Phonon Modes in Germanium Nanowires. *J. Appl. Phys.* **2007**, *102*, 014304.